Cathode-fall development in low-pressure, parallel-plane hydrogen discharges

B. M. Jelenković* and A. V. Phelps
JILA, University of Colorado and National Institute of Standards and Technology, Boulder, Colorado 80309-0440
(Received 24 May 1995; revised manuscript received 10 October 1995)

The temporal and spatial development of the cathode fall in pulsed, low-pressure hydrogen discharges is investigated using correlated measurements of the current, voltage, and optical emission. The results include the variation of relative emission probabilities versus time and position for the $H(n = 3)$ and $H_2(a^3\Sigma)$ states. The behavior of the higher-energy electrons is inferred from the first negative band emission of N_2^+ in mixtures of 2–3% N_2 in H_2. Measurements are reported for final, i.e., quasi-steady-state, discharge currents of 10–100 mA for pressure times electrode spacing (pd) values of 1 and 3 Torr cm, where 1 Torr = 133 Pa. The breakdown electric field E to gas density values vary from 1 kTd to 400 Td, where 1 Td = 1×10^{-21} V m^2. The H_α and the near-uv continuum emission data show the importance of heavy-particle excitation in the cathode-fall region. Representative transient current and voltage wave forms during the development of the cathode sheath are analyzed in terms of discharge and circuit parameters. During the period of rapid current growth at 3 Torr cm, transient emission wave forms for the uv continuum near the anode show a sudden drop that results from the collapse of the electric field.

PACS number(s): 52.80.Dy, 52.80.Hc, 52.40.Hf

I. INTRODUCTION

We present correlated spatial and temporal distributions of optical emission and of transient voltage and current wave forms in cathode-dominated, low-pressure discharges in H_2. In addition, we interpret the results in terms of the dominant collision processes and space-charge electric field distributions so as to make connections to previous work and to guide modelers as to important features and previously omitted processes. For example, spatially dependent transients and time-dependent spatial profiles of emission from atomic and molecular hydrogen are used to show that heavy-particle excitation needs to be added to cathode-fall models. Detailed comparisons of experiment with theory are left to researchers with better models than we have developed. We have chosen to work with H_2 because of the absence of long-lived metastable atoms and molecules. The price paid for this advantage is that the models must deal with three positive ions [1,2], i.e., H^+, H_2^+, and H_3^+, as well as two fast neutral species, i.e., H atoms and H_2 molecules formed in charge transfer collisions.

Numerous experimental and theoretical investigations have been made of the cathode regions of glow discharges [3,4]. These include measurements of the visual dimensions of emission patterns and of operating voltages [3–5], the electric field variation with distance from the cathode [6–10], voltage-current characteristics of diffuse and constricted discharges [11–13], and transient behavior of discharges and development of cathode fall [2,7,14,15]. Here we have emphasized references concerned with hydrogen discharges, where available. Many approaches have been developed for modeling charged-particle motion in the presence of the rapidly varying electric field of the cathode fall, e.g., the electron and ion behavior in both cathode sheath and negative glow [2,16–18]. The techniques used include the continuum or fluid model [14,19], the moment method [20], Monte Carlo simulation [21], particle-in-cell models [22], and the convective scheme [23].

Much of the work on low-pressure, pulsed discharges in H_2 has been motivated by high voltage switching and fusion applications [2,7,16,24–26]. Although relatively little research has been done for dc glow discharges in hydrogen or hydrogen mixed with other gases for plasma processing of materials, the importance of hydrogen is increasing because of its presence in rf discharges used in the deposition of hydrogenated amorphous silicon [27] and diamond films [28]. Models of the optical emission often used as a diagnostic for plasma processor discharges [29] generally assume that the observed excitation is only produced by electrons. We will show that this assumption is not valid for discharges with significant cathode fall voltages, e.g., sputtering discharges or rf discharges with large asymmetries.

Previous research on pulsed discharges in hydrogen includes that of McClure and co-workers [2], who conducted experimental and theoretical investigations of such discharges operating pressure p times electrode spacing d values of 0.5–2 Torr cm and at 40–80 kV, i.e., at several hundred times breakdown [30]. Measurements of current, spatially dependent H_β emission, and electric-field-induced Stark splitting of H_β lines using fast-rise-

*Permanent address: Institute of Physics, P.O. Box 57, Belgrade, Yugoslavia. Also at Time and Frequency Division, National Institute of Standards and Technology, Boulder, CO 80303.

time discharge voltages with 5–10 times the breakdown voltage were made by Nahemow, Wainfan, and Ward [7] over a wide range of *pd*. They found rough agreement between experiment and theory. Particularly evident was the development of the cathode fall via an ionization wave moving toward the cathode in times short compared to ion transit times. Later models of high-voltage pulsed breakdown in H_2 for *pd* values from 0.25 to 0.75 Torr cm by Lauer, Yu, and Cox [16] confirmed the general features of early experiments, but still yielded only approximate agreement for quantities such as breakdown voltages. Measurements and models of current growth were found by Schlumbohm [31] to agree very well for a constant and very low overvoltage ($< 10\%$) at $pd = 1$ Torr cm. No spatially dependent information was obtained. The present experiments complement the previous experiments in that they provide transient and steady-state voltage and current data and spatial distributions of emission throughout the transition from voltages below breakdown to above breakdown. In order to work in this region it is necessary to use an external circuit with a significant series resistance. The effects of such a circuit on the discharge must be taken into account when analyzing the data, whereas in the constant voltage experiments one can often neglect the details of the external circuit.

All of the models developed for hydrogen discharges [1,2,7,16,24–26,31–33] show the complexity of these discharges resulting from the multiplicity of ion species. Several authors [1,8] have discussed the composition of the space charge, e.g., the contribution of atomic and molecular ions at the cathode of hydrogen discharges. Dexter, Farrell, and Lees [1] made experimental determinations and Monte Carlo simulations of energy spectra and the relative fluxes of H^+, H_2^+ and H_3^+ in a discharge at 4 Torr cm and current density of 1.1 mA/cm^2. Hantzsche [1] calculated a flux density of neutral atoms and molecules 1–10 times larger than that of ions. Information regarding the velocity distributions of excited H atoms has been used to improve models of ion and fast atom behavior in the high electric fields typical of those found in the vicinity of the cathode fall in a dc hydrogen discharge [32,34].

An important question in the interpretation of experiments such as those of this paper is whether or not lateral constrictions of the discharge are present. Although constrictions in steady-state H_2 discharges dominated by the cathode fall have been reported [35,36], the constriction models developed thus far for hydrogen are simplified, single-ion models [37]. Experiments on constricted hydrogen glow discharges showed that the discharge obeys the similarity principle, e.g., the scaling of the discharge voltage versus j/p^2 [35]. Here j is the discharge current density and j/p^2, along with *pd*, is a scaling parameter appropriate to these discharges [3,4]. We will note when constrictions are expected to occur [36] in the present experiments.

The experimental observations of the transient current, voltage, and photon emission reported here extend from low currents, for which there is negligible field distortion, to high currents, for which the cathode sheath is highly developed and the electric field is expected to be highly distorted. The *pd* values used are 1 and 3 Torr cm so that the cathode-fall thickness is about equal to or less than the electrode separation [3,4]. The spatial distribution of processes responsible for the cathode fall is inferred from measurements of the optical and near-uv emission. We have measured spatial scans of Balmer alpha (H_α) and the near-uv continuum at different times during the cathode-fall development, i.e., from times before the space-charge distortion of the electric field to times after the high-current, steady-state cathode fall has been fully developed. The hydrogen transitions used have different energy dependences and thresholds for their electron excitation cross sections [38] and can be used to monitor temporal and spatial variation of different parts of the electron energy distribution function.

Because heavy-particle excitation [32,33] of hydrogen can exceed the electron excitation [39] throughout much of the gap, we have developed a more direct way of observing the effects of electron excitation. Transient measurements [40] of optical emission in low-current, pure-N_2 discharges at very high electric field to gas-density ratios E/n in pure N_2 have shown that the $N_2^+(B\,^2\Sigma_u \rightarrow X\,^2\Sigma_u^+, v'' = 0 \rightarrow v' = 0)$ transition of the first negative (1N) band near 391.4 nm is excited only by electrons. Upper atmosphere studies have often made use of the high ratio of electron excitation to proton excitation [41]. The predominance of electron excitation can occur because the cross sections for exciting the 1N transition by hydrogen atomic ions and neutral atoms in collisions with N_2 are small at the energies of interest here [42], e.g., a factor of 30 smaller than for electron excitation of N_2 at a laboratory energy of 200 eV. We have not found data for the excitation of the 391.4-nm band of N_2 in collisions of nitrogen ions or of neutral species with H_2. Because the cross section for electron excitation of the 391.4-nm band peaks at near 100 eV [43], measurements of the spatial and temporal behavior of the 1N band follow the behavior of the higher-energy (30–200 eV) electrons.

The experimental arrangement used in these experiments is reviewed in Sec. II. Section III contains steady-state voltage current data and Sec. IV presents transient voltage and current data obtained for 1 and 3 Torr cm. The instantaneous spatial distributions of relative emission are given in Sec. V. The results are discussed in Sec. VI. The present series of experiments also included absolute emission intensity determinations for steady-state hydrogen discharges that will not be reported here [44].

II. EXPERIMENT

The measurements are made in a discharge tube consisting of two parallel-plane electrodes surrounded by a closely fitting quartz cylinder used to prevent long path breakdown and allow operation of discharges at low *pd*, i.e., on the left-hand side of the Paschen curve [3]. The high-voltage electrode is the cathode in the present experiments and is 78 mm in diameter. The cathode is made of gold-plated copper. The anode material is gold

plated onto copper or stainless steel unless otherwise stated. Vacuum-grade graphite, with its low backscattered and secondary electron yields [45], is used for the central 60-mm-diam section of anode for some experiments. The quartz rests on the anode surface and its inner diameter (80 mm) determines the effective area of the anode. The spacing between electrodes is 1.05 cm. In the remainder of this paper the electrode separation is rounded off to 1 cm to give *pd* values of 1 and 3 Torr cm. Further details of the discharge tube, the vacuum conditions, cathode treatment, and pressure measurements have been given in earlier papers [36,46]. For example, because of the short H_2 metastable lifetimes and short duration experiments, gas phase collisions with impurities are not expected to be significant. On the other hand, changes in the cathode surface condition can be large. After aging the cathode, we were able to run a hydrogen discharge at pulsed currents of 50 mA many days with only moderate changes of discharge voltage ($\pm$ 15 V) and without significant additional sputtering of cathode material onto the quartz cylinder.

The electronic circuit used to superimpose the high-voltage pulse ($\leq$ 1.2 kV) on the dc voltage ($\leq$ 1 kV) so as to cause a transition from a low-current ($\leq$ 100 μmA) "keep alive" discharge to a high-current (10–100 mA) discharge is shown on Fig. 1. The dc discharge present between pulses operates at voltages slightly below the breakdown voltage V_B [30]. The breakdown voltages are $\approx$ 340 V and $\approx$ 470 V for *pd* values of 1 and 3 Torr cm, respectively [36,46,47]. When driven by pulses ($\approx$ 20 V), the high-voltage, metal-oxide-semiconductor field-effect transistor (MOSFET) effectively connects the 15-μF storage capacitor to ground. Voltage pulses of up to 1200 V, with measured rise times of about 100 ns followed by an overshoot $\approx$ 15%, lasting about 50 ns, are obtained at the junction of R_1 and R_2, i.e., at point A. The voltage generated at this point is applied to the discharge tube and its cable and electrode capacitance C_d (not shown separately in Fig. 1) through the series resistor R_2. The duration of the voltage pulses is normally less than 100 μs at a repetition rate of 3 Hz. When the pulse length is increased further, the voltage decreases with time because of charge drained from the storage capacitor. This pulsed-discharge technique [11,46] has an advantage over a continuous dc discharge because it minimizes gas and electrode heating, reduces sputtering of the cathode, and simplifies the measurement of the differential voltages in the presence of drifting breakdown voltages.

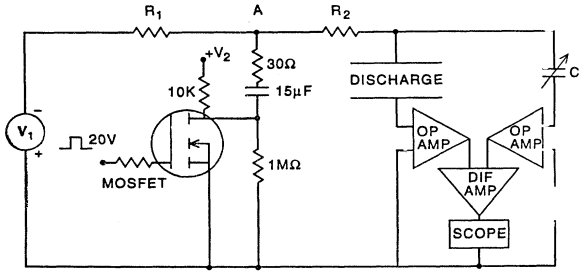

FIG. 1. Schematic of the circuit for pulsed discharge experiment. The resistor R_1 is typically 20 kΩ and the discharge "series" resistor R_2 is varied from 10 kΩ to 5 MΩ. The dc voltages V_1 and V_2 determine the current between pulses and the magnitude of the voltage pulse at point A, respectively. OP AMP and DIF AMP stand for the operational amplifier and differential amplifier discussed in the text.

The bridge circuit between the discharge and ground shown in Fig. 1 is used to cancel the displacement current flowing between the discharge electrodes and to allow measurement of only the discharge current. The variable capacitance is adjusted to give no signal from the differential amplifier in the absence of a discharge. As in previous experiments [46], the operational amplifier used to measure the discharge current reduces the impedance between the anode and ground to essentially zero. We use a fast voltage probe ($\approx$ 80 MHz bandwidth when matched to the oscilloscope) for measuring the discharge voltage transient. The current and voltage transients are recorded using a 100-MHz storage scope and then are transferred to a personal computer. The voltage scale of the oscilloscope-computer combination was calibrated against a precision voltage supply. Resistors known to better than $\pm$2% were used to determine the current. However, it was necessary to apply a correction factor to some of the current data [48].

The measurements of H_α, near-uv continuum of H_2, and N_2^+ first negative band emission are made with interference filters centered at 656.2, 200, and 391 nm [49], respectively. Each filter had a full width at half maximum of 10 nm [50]. The light is detected using a photomultiplier with a multialkali photocathode that is listed as sensitive from 185 to 930 nm. The collimator and quartz lens system [51] has a spatial resolution $\approx$ 1 mm. Loss of resolution at positions near the electrodes, caused by shielding of the discharge by the electrodes, is reduced by using a small optical aperture at the lens. The transient measurements cited as near the cathode or anode are taken at approximately 1 mm from the respective electrode. Saturation of the photomultiplier at high discharge currents is avoided by inserting a neutral density (ND1) filter.

The optically produced current transients from the photomultiplier are amplified using a 200-MHz amplifier and recorded using a 100-MHz storage scope. These data are corrected for the measured delay of 30 ns. Spatial scans of optical emission at different times during the development of the cathode fall are recorded using a boxcar gate that is delayed relative to the start of the voltage pulse. The boxcar gate widths are $\sim$ 0.1 μs at times near the peak current and $\approx$ 2 μs for the quasi-steady-state data. These data have been normalized to the boxcar gate length and to changes in quasi-steady-state current. The output of a second boxcar that samples the emission during the quasi-steady-state portion of the current pulse is used to correct for drift in the discharge current. For the spatially dependent emission at low dc currents, the photomultiplier output is recorded using a gated (30–50 ms) photon-counting chain and a 100-MHz scaler. The spatial scanning is done by moving the photomultiplier on the computer-controlled table described in Ref. [46].

III. STEADY-STATE VOLTAGE AND CURRENT

We first present the measured quasi-steady-state voltage-current characteristics for low-pressure, parallel-plane discharges in H_2 shown in Fig. 2 at the pressures used in our experiments. The plot includes data from the present experiments as well as from earlier measurements with the same apparatus [36,46]. We have not plotted voltage versus the scaling variable j/p^2 [3,4,11,12,36,46] because some of the data are for constricted discharges with an unknown effective discharge area. At very low currents, for which aging of the cathode is slow, the data are obtained with dc operation of the discharge. At currents above about 100 μA, the pulse technique of Sec. II is generally used to minimize errors caused by drift in the discharge operating voltage. The low-current, dc discharges supply initiating electrons for the pulsed discharge and appear visually to be radially diffuse [36,47]. Note the spread ($\approx$ 30 V) in measured voltages in spite of several hours of aging of the discharge electrodes and the use of fresh charges of gas. The regions of positive slope to the V-I data of Fig. 2 are conventionally [3,4] labeled as the "abnormal discharge" regions because the current densities are above the "normal" current density. The normal current density is that for which increasing the current through a constricted discharge causes the glowing region to just fill the electrode area [3,4].

We next present representative current and voltage transients for pulsed discharges at 3 and 1 Torr and discuss their interpretation. We then summarize the measured spatial distributions of emission and discuss their relation to the current and emission transients.

IV. TRANSIENT VOLTAGE, CURRENT, AND EMISSION

The experimental time development of the voltage across the discharge, the current through the discharge, and the uv emission are shown by the wave forms (solid lines) of Figs. 3 and 4 for pressure times electrode spacing values of 3 and 1 Torr cm. Figures 3(a) and 4(a) show the voltage applied to point A in Fig. 1 as well as the voltage across the discharge. Figures 3(b) and 4(b) show the discharge current and Figs. 3(c) and 4(c) show the H_2 near-uv continuum from positions near the cathode and near the anode. The behaviors of the voltage and current transients for the two pressures are qualitatively similar, but on a rather different time scale. The emission transients from near the anode are very different.

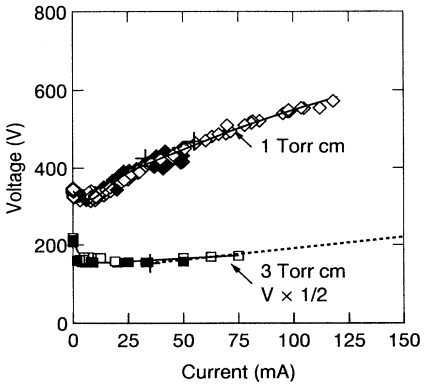

FIG. 2. Quasi-steady-state voltage-current characteristics for hydrogen for pd values of 1 Torr cm (diamonds) and 3 Torr cm (squares). The solid symbols are for a graphite anode and the open symbols are for a gold-plated copper anode. The solid curves are rough averages through the data. The dotted lines, with their end points indicated by crosses, are calculated from the approach of the transient voltage and current to their steady-state values as shown in Figs. 3 and 4.

A. Voltage and current transients

The voltage applied to the discharge circuit consists of a dc voltage that maintains a low current (1–100 μA) and a pulse that raises the discharge current to values sufficient to establish a cathode fall. Previous work has shown that these dc, low-current discharges operate at a voltage just below the breakdown voltage [36,46,47]. On the time scale of the plots of Figs. 3 and 4, the voltage pulse applied at point A in Fig. 1 and superimposed on the dc voltage is effectively a step function beginning at $t = 0$. The discharge voltage initially increases linearly as the circuit capacitance is charged and then drops as the circuit capacitance, i.e., the electrode plus wiring capacitance C_d, loses charge through the discharge. In Figs. 3(a) and 4(a) the rising dot-dashed curve

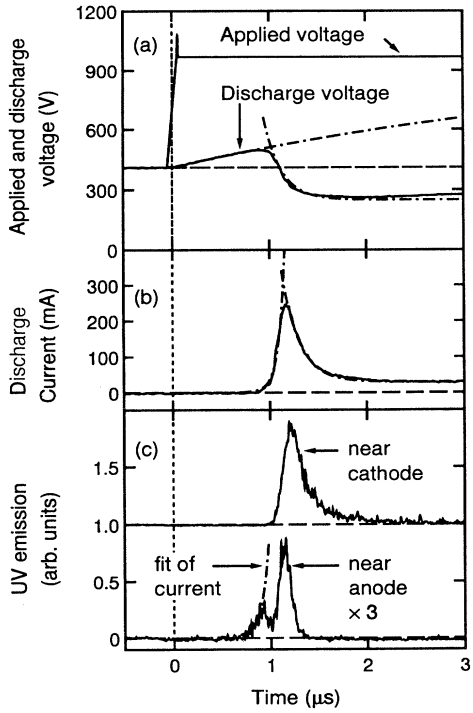

FIG. 3. (a) Applied voltage and discharge voltage, (b) current wave forms, and (c) discharge emission from near cathode and anode for 3 Torr cm. The solid curves are from experiment and the dot-dashed curves are fits to the data discussed in the text.

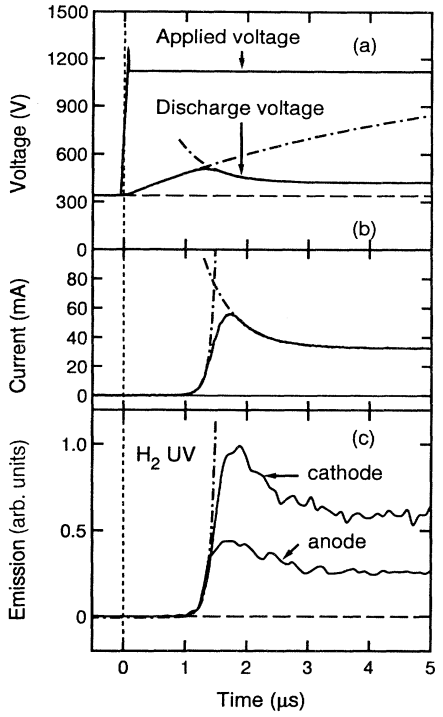

FIG. 4. (a) Applied voltage and discharge voltage, (b) current wave forms, and (c) discharge emission from near cathode and anode for 1 Torr cm. The solid curves are from experiment and the dot-dashed curves are fits to the data discussed in the text.

is calculated using the experimental time constant determined by the circuit capacitance ($C = 250$ pF) and the series resistance of $R_2 = 20$ kΩ and gives the voltage that would be present in the absence of a discharge. The magnitude of the calculated voltage pulse shown is adjusted to fit the initial rise of discharge voltage, because very few measurements were made of this voltage pulse. The falling dot-dashed curves are fits of exponential decays to the measured voltages as they approach steady state. The effective differential resistance values calculated from these measured time constants and the circuit capacitance are plotted as dotted lines in Fig. 2. In the 1-Torr cm case the dotted line is not distinguishable from the data points. The good agreement of the transient data with the dc results indicates that once the cathode fall is established the response time of the discharge is well below the measured time constants of about 0.5 μs.

The discharge currents are shown in Figs. 3(b) and 4(b). The displacement current flowing through the discharge region as the result of the voltage changes across the discharge tube is balanced out by the bridge circuit of Fig. 1, so that the observed current is that produced by the motion of charged particles and changes in electric fields within the discharge. The initial discharge current has been shown to increase exponentially with the square of time as long as the currents are low enough so that the electric field is spatially uniform and increases linearly with time [46,47]. The increasing dot-dashed lines in Figs. 3(b) and 4(b) show comparisons of the later portion of this current-growth model with experiment (solid curve). Thus the large delays (≈ 1 μs) in the current buildups occur as the current increases from the prepulse values of 30–100 μA to values of the order of 10 mA, where space-charge effects are calculated to become significant [47]. The normalized rates of current growth calculated from these fits to the rising current scatter around previous results [46,47].

As the discharge capacitance loses its charge, the discharge voltage and current drop to the quasi-steady-state values. The exponential behavior of the approach to steady state is indicated by the decreasing dot-dashed curves in the current wave forms of Figs. 3(b) and 4(b). Here the time constants used in the fits are the same as for the respective voltage wave forms. The shape of the current and voltage wave forms near peak current and the final values of the currents are found not to change with the magnitude of the initial current, although the delay in current growth decreases with increasing initial current because of the smaller buildup required. Note that a good estimate of the current wave form can be obtained by drawing a smooth curve between the asymptotic current-rise and current-fall curves.

The voltage changes from the prepulse discharge voltages to the quasi-steady-state voltages are positive for 1 Torr cm and negative for 3 Torr cm and are consistent with the data of Fig. 2. Models for the increased efficiency and lower operating voltages below breakdown of these hydrogen discharges, i.e., the negative differential voltages portions shown in Fig. 2, have recently been discussed [47,52]. The reasons for the minimum in the voltage at about 2 μs for 3 Torr cm are unknown. At 3 Torr cm and "final" currents of $\sim$ 10 mA, for which the steady-state discharge has been found to be constricted [36], there is often additional structures in the current wave form at times of the order of 20 μs that can take the form of damped oscillations. This observation suggests the possibility of rotational motion [53] or of "radial-breathing" [54] motion of the region of high ionization and emission, leading to constriction. We suggest that during the times shown in Fig. 3 the discharge retains the initial diffuse distribution across the cathode characteristic of the very low currents prior to the pulse. The discharge then constricts at or after the times of the structure or oscillations. Further observations would be necessary to confirm this hypothesis. Such behavior has been observed experimentally in Ar discharges [53].

B. Emission transients

Shown in Figs. 3(c) and 4(c) are H_2 uv continuum emission wave forms from positions near the cathode and anode (solid lines). The dot-dashed curves are magnifications of the calculated current wave forms from Figs. 3(b) and 4(b), respectively. As discussed previously [36] for uniform electric field experiments, the emission near the cathode is the result of excitation by fast H atoms produced in collisions of H^+ with H_2 and with the cathode, whereas the emission from near the anode is expected to be from both fast H atoms backscattered from the cath-

ode and from electron impact excitation of H_2.

For the 3-Torr cm data of Fig. 3 the uv emission near the anode follows the current (dot-dashed curve) as long as the electric field is essentially uniform, i.e., until the discharge current reaches about 10 mA or 200 $\mu A/cm^2$. The decrease of this uv emission beginning at 1.7 μs is interpreted as a result of the decrease of electric field near the anode that occurs with the redistribution of charge. The redistribution of electric field ultimately results in the formation of the quasineutral low-electron-energy plasma between the negative glow and the anode, known as the "Faraday dark space" [3,4]. The rise in uv emission near the anode beginning at 1.9 μs follows the current growth through the spatially stable plasma between the negative glow and the anode. These changes are qualitatively similar to the time dependence of emission typically observed in the early afterglow of pulsed discharges [55] as the electrons cool and then recombine with ions. The uv emission near the cathode continues to increase with current throughout this time period. However, when the peak of emission from the cathode region is normalized to the peak current, the emission is observed to be delayed relative to the current by about 100 ns. This time is more than an electron transit time but less than ion transit times inferred from transient measurements at low currents [53]. This delay suggests that the excitation results form heavy particles produced close to the cathode. The much higher magnitude of the uv emission near the cathode will be discussed further in Sec. V A 3.

For 1 Torr cm the structure in the transient uv emission from near the anode shown for 3 Torr cm in Fig. 3 is replaced by an early leveling off of emission shown in Fig. 4(c). This observation supports the previous suggestion [3,4,9] that the decrease in electric field near the anode is small when the electrode separation is comparable with the nominal cathode-fall thickness, i.e., when the discharge is partially "obstructed." The uv emission from near the cathode follows the discharge current rather closely.

The H_α emission transient and the rather noisy 1N emission transient (neither shown) for 3 Torr cm and the current pulse of Fig. 3 show a decrease in their rates of growth beginning at the same time (1.7 μs) as the structure in the uv continuum emission. These wave forms then increase monotonically to their peak values. The reduced rate of rise in these cases is consistent with the decrease in the flux of high-energy electrons that occurs near the anode with the redistribution of the electric field [3,4].

V. SPATIAL DEPENDENCE OF EMISSION

In this section we present measurements of the spatial dependence of optical emission at various times during the development of the cathode fall for *pd* values of 3 and 1 Torr cm. We interpret the data in terms of the dominant discharge and collisional excitation processes. The simplest data set to interpret is the 1N emission from N_2^+ and we present it in Figs. 5(a) and 6(a). This is followed by the H_α emission data [Figs. 5(b) and 6(b)] and the uv continuum emission data [Figs. 5(c) and 6(c)], respectively. The insets to Figs. 5(b) and 6(b) show the current wave form for the two series of data and show the times at which the various numbered spatial profiles were recorded. The reproducibility of the spatial scans is about ± 10%.

The spatial scans obtained during the pulsed discharge are labeled as curves 2–5 in Figs. 5 and 6 and are measured using the boxcar circuit described in Sec. II. The data points and smooth curves associated with curves 2–5 of each panel are normalized to a common scale of relative intensities. The spatial scans obtained at the very low, predischarge current levels (curves 1) are actually measured using a dc discharge and the counting technique for recording the photomultiplier output. The scale factors applied to the data points and smooth curves associated with curves 1 are arbitrary.

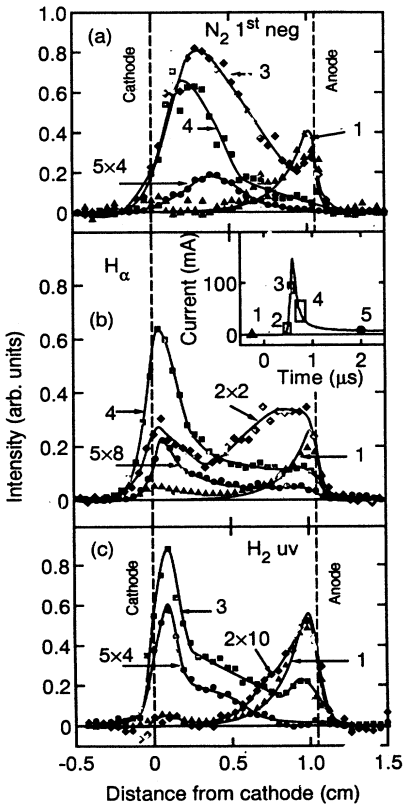

FIG. 5. Spatial scans of the (a) first negative band of N_2^+ emission, (b) H_α emission, and (c) H_2 near-uv continuum emission for 3 Torr cm. Curves 2–5 show the spatial scans at different times during the development of the cathode fall of a pulsed discharge in H_2. The notation 5 × 4 means that the relative emission data for curve 5 has been multiplied by a factor of 4 before plotting. Curve 1 shows a fit of the calculated spatial dependence in the absence of space charge to data from low-current, dc experiment (triangles). Curve 1 and the associated data points are plotted on an arbitrary scale. The inset to panel (b) shows the current transient and the times at which the spatial scans are made.

A. Spatial scans for 3 Torr cm

The observations of temporally and spatially resolved emission for $pd = 3$ Torr cm presented in this section provide a detailed description of the development of the cathode glow in a case where the cathode-fall thickness is significantly smaller than the separation of the electrodes. These data demonstrate the importance of excitation of hydrogen by heavy particles during cathode-fall development and in the steady state. In addition, the discharge apparently becomes constricted at longer times than those reported here, i.e., we are examining a previously unreported "metastable" state of the hydrogen discharge. The constrictions have been observed directly by Petrović and Phelps [53], who found that for currents from ≈ 2 mA to ≈ 40 mA the emission observed through a semitransparent anode is concentrated near the quartz wall of this discharge cell. Unpublished results [56] for currents below 10 μA, $pd = 2$ Torr cm, and the quasi-steady-state portion of the pulse show nearly uniform discharges across the cathode. However, significant asymmetry is observed at $pd = 0.5$ and 4 Torr cm [56]. No current dependence is found for less than 10 μA.

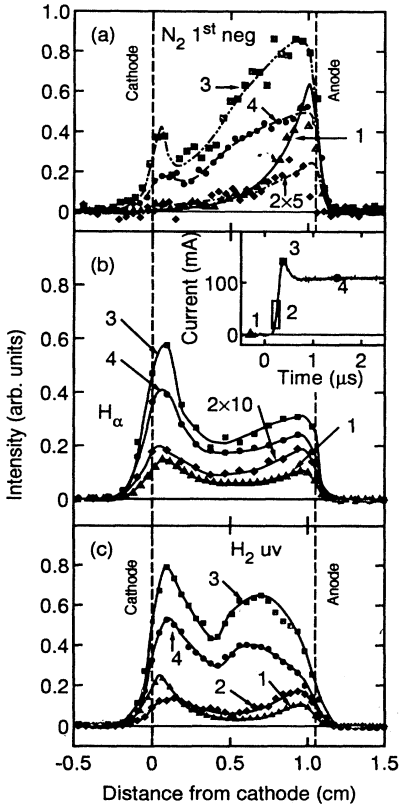

FIG. 6. Spatial scans of the (a) first negative band of N_2^+ emission, (b) H_α emission, and (c) H_2 near-uv continuum emission for 1 Torr cm. Curves 2–4 show the spatial scans at different times during the development of the cathode fall of a pulsed discharge in H_2. The notation 2×10 means that the relative emission data for curve 2 has been multiplied by a factor of 10 before plotting. Curve 1 shows a fit of the calculated spatial dependence in the absence of space charge to data from low-current, dc experiment (triangles). Curve 1 and the associated data points are plotted on an arbitrary scale. The inset to panel (b) shows the current transient and the times at which the spatial scans are made.

1. *First negative band emission from N_2-H_2 mixtures*

The spatial variations of the relative 1N emission obtained during the current buildup, near current maximum, and during the quasi-steady-state discharge are shown in Fig. 5 by diamonds (curve 3), squares (curve 4), and circles (curve 5), respectively. The data values shown in Fig. 5 are the differences between signals obtained with the 3% N_2-H_2 mixture and with pure H_2 so as to subtract out the moderately strong background signal near 391.4 nm. These background signals probably result from excitation of the uv continuum of H_2 by fast H atoms [32] and by electrons [39]. Smooth curves are drawn through these sets of data points to aid the eye. Curves 3, 4, and 5 are plotted to the same intensity scale. The relationship of the emission signal to the instantaneous current indicated at points 2 or 3 of the current transient is subject to considerable uncertainty because of uncertainties in the recording of the timing of the boxcar gate.

The results of the axial spatial distribution of 1N emission of N_2 from N_2-H_2 mixtures when the current reaches the quasi-steady-state value of 10 mA presented in curve 3 in Fig. 5(a) show that the electron excitation peaks at about 3 mm from cathode. The spatial scans also show that the distance from the cathode to the position of maximum emission, which we define as the length of cathode fall [57,58], decreases as the cathode fall forms and then increases as the current decreases toward the steady-state value. The minimum cathode-fall length occurs shortly after the current maximum. The increasing cathode-fall distance with decreasing current is characteristic of steady-state models of the cathode fall [3,4].

It is unlikely that electron backscattering [46] plays a significant role in the production of 1N excitation at 3 Torr cm even for the gold-on-copper anode of these runs. Therefore, it is not surprising that the exponential increase of the 1N emission observed at very low currents yields an ionization coefficient of 5×10^{-21} m^2, in good agreement with previous measurements [59,60]. The calculated exponential growth curves [curves 1 of Figs. 5(a) and 6(a)] have been rounded near the electrodes to simulate the effects of the finite spatial resolution of the detection system.

2. *Balmer α emission*

The measured spatial variations of H_α emission at various times during the current transient are shown in Fig. 5(b). These spatial scans are most notable for the large emission signals that peak at the cathode to within the spatial resolution of the apparatus. We attribute these peaks to the recently proposed excitation

of the H_α transition by fast H atoms produced in H^+ charge transfer collisions with H_2 and with the cathode [32]. The relative increase in H_α emission near the cathode with the development of the cathode fall shown in Fig. 5(b) is interpreted to be the result of an increase of the electric field in the cathode vicinity that produces higher energy ions and, by charge transfer and surface collisions, higher-energy H atoms. Note that if curves 4 and 5 of Fig. 5(b) were normalized to their respective instantaneous currents there would be an intermingling of points near the anode where electron excitation dominates, i.e., these emission signals are proportional to their respective discharge currents. This kind of comparison is not possible for curve 2 because of uncertainties in the timing of the boxcar gate.

Because ion energies are small near the anode, we interpret the broad peak near the anode shown by curve 2 for the H_α emission as resulting from electron excitation. By the time of points 4 and 5 the electron excitation is only a weak shoulder on the corresponding H_α profiles.

3. Ultraviolet continuum emission

Shown in Fig. 5(c) are spatial scans of uv emission taken at times in the development of the cathode fall shown in the inset of Fig. 5(b). The difference between the spatial distribution of emission just as the current becomes noticeable (diamonds and curve 2) and from a low-current, steady-state diffuse discharge at 10 μA (triangles and curve 1) shows the onset of space-charge effects, e.g., the beginning of a cathode-glow-like emission maximum at about 0.7 cm from the cathode. The spatial distribution of uv emission near the cathode obtained just prior to the current peak (curve 3) is very similar to the emission from the quasi-steady-state discharge at 10 mA near the end of the current transient (curve 5). It takes less than 100 ns, i.e., from point 2 to point 3 on the transient-current wave form, for the spatial dependence of emission to reach the distribution characteristic of the quasi-steady-state as shown in curve 4. The emission peak in the region of high electric field near the cathode may be caused by fast H atom excitation of the $H_2(a\,^3\Sigma)$ state [33], but no information is available as to the cross section for this process. The contribution of electron excitation in the negative glow that was seen so clearly in curve 5 of Fig. 5(a) appears only as a shoulder at about 4 mm from the cathode in curves 3 and 5 of Fig. 5(c). Note that these spatial scans are not sufficiently close in time for us to detect the minimum in the uv continuum that was found in the emission transient from near the anode in Fig. 3(c).

B. Spatial scans for 1 Torr cm

The behavior of hydrogen discharges at 1 Torr cm is significantly different from that at 3 Torr cm. For example, we will show that in the 1-Torr cm case the maximum of emission corresponding to the cathode glow is much more difficult to detect. Also, the maximum in the uv continuum emission near the cathode is much less pronounced than in the 3-Torr cm case in spite of the larger cathode-fall voltage. Another important aspect of the 1-Torr cm data is the very noticeable effect of changing the anode material that is attributed to changes in electron backscattering. Note that because of changes in the pulse voltage and the series resistor, the quasi-steady-state current for Fig. 6 is much larger than for Fig. 4.

1. First negative band emission from N_2-H_2 mixtures

The spatial variations of the relative 1N emission obtained early in the current buildup, near current maximum, and during the quasi-steady-state discharge are shown in Fig. 6 by the points associated with curves 2, 3, and 4, respectively. Again, the data values shown in Fig. 6(a) are the differences between signals obtained with the 3% N_2-H_2 mixture and with pure H_2. Curves 2–4 are plotted to the same intensity scale. The corresponding times are indicated on the current wave form shown in the inset of Fig. 6(b). For the low currents of curve 1, the electric field calculated from the model of Ref. [47] (Sec. IV A) and from measured average ion transit times [53] is found to be spatially uniform to within 0.5%.

The spatial dependence of the 1N emission at low dc currents is in good agreement with an exponential growth (solid curve 1). The spatial ionization coefficient determining the exponential growth is adjusted for a good overall fit to the low-current emission data. These spatial ionization coefficients compare well with other values [39,60,44] at the corresponding E/n. The observed exponential increase of the optical signal with distance over most of the gap for this pd is consistent with measurements of discharge current versus electrode separation [59]. The increases in emission shown by curves 3 and 4 relative to curve 1 for distances between 0.2 and 0.8 cm from the cathode are evidence that the electric field has increased significantly toward the cathode. However, there is not sufficient space-charge distortion of the electric field to cause a maximum in the light output, such as is attributed to the presence of a cathode glow. These results are consistent with the published values [3,4] for the normalized thickness of the cathode fall $\approx$ 0.8 Torr cm, for H_2 discharges at j/p^2 of 0.2–2 mA/cm^2 Torr^2. Therefore this discharge is classified as an obstructed discharge because the cathode-to-anode distance is too small for a full cathode-fall negative glow region to develop [3,4]. A direct measurement of the electric fields for an obstructed discharge in H_2 is that of Ganguly and Garscadden [9]. In this paper small departures from an axially uniform electric field were found for lower pd, 0.2 Torr cm, at approximately the same current density.

The reason for the peaks in 1N emission near the cathode seen in curves 3 and 4 of Fig. 6 is unknown. Because the data are the differences between signals obtained with the 3% N_2-H_2 mixture and with pure H_2, the moderately strong background signal near 391.4 nm from pure H_2 should have been subtracted out. Note that the peaks shown become larger as the field near the cathode increases, as expected for heavy-particle excitation. The

next subsection addresses the strong heavy-particle effects in H_α emission. Because low signal levels limited the useful resolution of the monochromator, we were unable to make spectral scans to determine whether the emission peaks near the cathode result from radiation from N_2 excited by H atoms and/or ions or from incomplete subtraction of the background H_2 emission.

2. *Balmer α emission*

The measured spatial variations of H_α emission at different times during the current transient are shown in Fig. 6(b). The spatial scans for the Balmer line are qualitatively similar to those of the 1N band for positions near the anode, but are very different near the cathode. The relative increase in H_α emission near the cathode with the development of the cathode fall shown in Fig. 6 is interpreted to be the result of an increase of the electric field in the cathode vicinity that produces higher-energy ions and fast neutral particles. Previous work [32] with spatially uniform electric fields has shown the heavy particle excitation to be particularly sensitive to the changes of the field at E/n near the present initial value of 1.1 kTd. The H_α emission from the present discharges is particularly strong and relatively free from noise and so should make a good diagnostic for testing models.

3. *Ultraviolet continuum emission*

The emission of H_2 uv continuum radiation is a useful diagnostic for comparing experiment and models because it is excited by relatively low-energy electrons [39] and apparently by fast ions, neutral atoms, or molecules [33]. The changes in the spatial distribution of uv emission with increasing current presented in Fig. 6 (curve 1 to curve 2) show a marked increase in relative uv production near the cathode, presumably from an increase in electric field and ion or neutral-species energy. After the discharge voltage starts to decrease from its maximum value Fig. 6 shows a further increase of current and a much greater distortion of the electric field is inferred from curve 3 compared to curve 2. There is little difference between the spatial dependence for data taken at the maximum of the current curve (curve 3) and that for data obtained during the steady-state discharge at 110 mA (curve 4).

The results presented in Fig. 6(c) indicate that the distance from the cathode to the maximum of emission is about 0.6 Torr cm, whereas the 1N data of Fig. 6(a) indicate 0.9 Torr cm. We attribute this difference to the fact that the anode material for the data of Fig. 6(c) is graphite, whereas that for Figs. 6(a) and 6(b) is gold-plated copper. Because the electron backscattering probabilities for graphite are smaller than for gold [45,51], the electron-induced excitation near the anode is significantly lower for the uv data than for the H_α line. Unfortunately, no 1N emission data with the graphite anode is available for $pd = 1$ Torr cm.

VI. DISCUSSION

Advances to the physics of low-pressure gas discharges presented in this paper are (a) making available of relative emission intensities from the dominant optical emission features as a function of time and position during the development of the discharge, (b) providing correlated emission and current transients, and (c) the qualitative discussion of the principal spatial and temporal features of the emission data that bring out the points of comparison with previous results and indicate desirable improvements in future models. Specific different features of the data include (a) the temporal development of the very strong emission from H_α and the near-uv continuum from positions near the cathode, (b) the resultant difficulty in using the common diagnostic of H_α emission as a measure of electron behavior in low-pressure, cathode-fall-dominated, H_2 discharges, (c) the utility of the first negative band emission of N_2^+ from small admixtures of N_2 in H_2 for monitoring the electrons in the cathode-fall region of H_2 discharges, (d) the previously ignored possibility of using the relatively intense near-uv continuum of H_2 as a discharge diagnostic, (e) the motion of the apparent negative glow toward and then away from the cathode during the cathode-fall development, and (f) the quasi-static approach of the discharge current to the final value. Further discussion of some of these features is given below.

The data of this paper show the development of the cathode fall after a voltage pulse is applied to a low-current diffuse discharge in a typical discharge circuit. It is convenient to divide the transition from low to high currents into two parts. The first period is the previously studied formative time lag and is characterized by low currents and small distortion of electric field. The length of this period depends on the time constant for the increase of voltage across the discharge, the current growth constant normalized to pressure as a function of E/n and pd, and the ratio of the initial and minimum observable values of the current [46,47]. This time interval is followed by a continued current increase and a voltage drop and then by a decrease in current to the quasi-steady-state value. The time constant for this decay of voltage and current is determined by the differential voltage-current ratio of the abnormal discharge and the circuit capacitance. This time constant and the value of the quasi-steady-state current do not change with the magnitude of the small current used to provide initiating electrons for the discharge growth. Our results can be compared with the current growth measurements for H_2 of Schlumbohm [31]. Because the series resistance was negligible in that experiment, the discharge voltage was constant during the current measurements, the formative time lags were short, the discharge voltages were always above breakdown, and the final currents were relatively large. By using a high external resistance we are able to work at voltages below breakdown in the region of the negative differential voltage-current characteristics and of constricted discharges. Although not pursued in this paper, such operation allows measurements during the development of constricted discharges.

By monitoring the H_α and H_2 uv emission from hydrogen and the 1N emission of nitrogen ion in a mixture of 2–3 % N_2 in H_2 we were able to observe both the electron and heavy particle excitation. This allows us to separate the effect of development of the cathode fall on electrons from its effect on ions and fast neutral atoms. Thus, for a pd of 3 Torr cm we found the expected evidence for large variations of the electric field due to space charge because the pd_c of the cathode fall is small compared with the pd of the discharge electrodes. At 1 Torr cm, the spatial distribution of the electron and heavy particle excitation per unit current and the spatial distribution of the electric field appear to be almost unchanged as the current is increased up to 100 mA (2 mA/cm^2). The electric field distortion is small because the value of pd_c for the cathode fall is comparable with the pd.

The H_α emission from these discharges is particularly strong, relatively free from noise, and makes a good diagnostic for testing models. Because of the large electron-excitation cross section for H_α at high energies, this emission is sensitive to the high-energy tail of the electron energy distribution. Similarly, the emission of the uv continuum radiation by H_2 is strong and can be made relatively more intense by the use of a detection system sensitive over as much as possible of the range from 170 to 330 nm. Because it is excited predominantly by electrons with energies near threshold, the uv continuum samples the low-energy portion of the electron energy distribution. Each of these emission features appears to be also excited by heavy particles, but very little is known about the magnitudes and energy dependences of cross sections at collision energies of interest here.

The measurement of 1N emission of nitrogen ions from a mixture of small concentrations of N_2 in H_2 proved to be a useful technique for monitoring the electron behavior in H_2 discharges. The technique was relatively inconvenient, however, because of the necessity of preparing the mixtures and because of the need to make background measurements using pure H_2. An alternative technique to be considered is to use a detection system with sufficient spectral resolution so as to observe the portions of the H_α line resulting from electron excitation [34,61,62]. A third technique might be to measure the emission from the $H_2(d\,^3\Pi_u)$ state [34]. The strong bands are located near 602 nm so that they are well separated from the uv continuum.

Spatial scans of 1N emission from admixed N_2 taken during the development of the cathode fall reveal the time variation of position of the negative glow, i.e., the position of maximum emission resulting from electron excitation. The distance to the position of maximum intensity in the negative glow decreases at high currents, with the shortest distance occurring soon after the maximum current. The steady-state results agree with some of the published data [5], but not with others [4]. The cases of disagreement may result from differences in experimental techniques, e.g., visual versus spectrally resolved measurements, and the different effects of heavy-particle excitation on various spectral features.

A source of confusion in the determination of electron behavior using emission is the excitation by electrons backscattered from the anode [45]. Fortunately, the high-energy maximum of the 1N excitation cross section minimizes this effect compared to, for example, the uv continuum emission with its low-energy excitation peak. The replacement of the gold anode with a graphite anode significantly reduces the number of backscattered electrons [38,51].

The data presented in this paper provide a number of measurements against which to test future models of low-pressure, parallel-plane hydrogen discharges, ranging from the development of space-charge electric fields and their effects on nonequilibrium electron motion to the previously undocumented excitation of the uv continuum by fast hydrogen ions or neutral species. Of course, these data are only a small part of that needed to cover all of the phenomena that occur in these discharges.

ACKNOWLEDGMENTS

The authors thank A. Gallagher and Z. Lj. Petrović for helpful discussions and J. D. Krakover for help with programming the personal computer. They particularly wish to thank T. Brown for the design and construction of the differential amplifier circuit. This work was supported in part by the Air Force Wright Laboratories, the National Institute of Standards and Technology, the U.S.–Yugoslav Joint Board (Project No. 924), and the Serbian Ministry of Science and Technology.

[1] R. M. Chaudrhi and M. L. Oliphant, Proc. R. Soc. London Ser. A **137**, 662 (1932); J. D. Craggs, Proc. Phys. Soc. London **54**, 245 (1942); K. Deutscher and D. Kamke, Z. Phys. **135**, 380 (1953); W. D. Davis and T. A. Vanderslice, Phys. Rev. **131**, 219 (1963); E. Hantzsche, Beitr. Plasmaphys. **9**, 439 (1969); V. S. Boldassov, A. I. Kuz'michev, and D. S. Fillipchev, Izv. Vyssh. Ucheon. Zaved. Radiofiz. **27**, 925 (1984) [Sov. Radiophys. **27**, 656 (1984)]; O. Fukumasa, R. Itatani, and S. Saeki, J. Phys. D **18**, 2433 (1985); A. C. Dexter, T. Farrell, and M. I. Lees, *ibid.* **22**, 413 (1989); V. P. Konovalov, J. Bretagne, and G. Gousset, *ibid.* **25**, 1073 (1992).

[2] G. W. McClure, Phys. Rev. **124**, 969 (1961); G. W. McClure and K. D. Granzow, *ibid.* **125**, 3 (1962); K. D. Granzow and G. W. McClure, *ibid.* **125**, 1792 (1962).

[3] M. J. Druyvesteyn and F. M. Penning, Rev. Mod. Phys. **12**, 87 (1940).

[4] G. Francis, Handb. Phys. **21**, 81 (1956).

[5] A. Gütherschulze, Z. Phys. **49**, 358 (1928); **61**, 1 (1930).

[6] R. Warren, Phys. Rev. **98**, 1650 (1955).

[7] M. Nahemow and N. Wainfan, J. Appl. Phys. **34**, 2988 (1963); M. Nahemow, N. Wainfan, and A. L. Ward, Phys. Rev. **137**, A56 (1965).

[8] R. Döpel, Beitr. Plasmaphys. **16**, 411 (1976).

[9] B. N. Ganguly and A. Garscadden, J. Appl. Phys. **70**, 621 (1991).
[10] C. Barbeau and J. Jolly, App. Phys. Lett. **58**, 237 (1991).
[11] B. N. Klyarfel'd, L. G. Guseva, and A. S. Pokrovskaya-Soboleva, Zh. Tekh. Fiz. **36**, 704 (1966) [Sov. Phys. Tech. Phys. **11**, 520 (1966)].
[12] M. Yumoto, N. Yamaoka, and T. Sakai, J. Phys. D **22**, 1856 (1989).
[13] V. N. Melekhin and N. Y. Naumov, Zh. Tekh. Fiz. **54**, 1521 (1984) [Sov. Phys. Tech. Phys. **29**, 888 (1984)]; V. N. Melekhin, N. Y. Naumov, and N. P. Tkachenko, *ibid.* **57**, 454 (1987) [*ibid.* **32**, 274 (1987)].
[14] A. Mitchell, G. R. Scheller, R. A. Gottscho, and D. B. Graves, Phys. Rev. A **40**, 5199 (1989); H. Debontride, J. Derouard, P. Edel, R. Romestain, N. Sadeghi, and J. P. Boeuf, *ibid.* **40**, 5208 (1989).
[15] R. Dreiskemper, G. Schroëder, and W. Bötticher, IEEE Trans. Plasma Sci. **23**, 180 (1995).
[16] E. J. Lauer, S. S. Yu, and D. M. Cox, Phys. Rev. A **23**, 2250 (1981).
[17] B. E. Thompson, K. D. Allen, A. D. Richards, and H. H. Sawin, J. Appl. Phys. **59**, 1890 (1986); J. Liu, G. L. Huppert, and H. H. Sawin, *ibid.* **68**, 3916 (1990).
[18] J. E. Lawler, Phys. Rev. **32**, 2977 (1985).
[19] P. Bayle, J. Vacquine, and M. Bayle, Phys. Rev. A **34**, 360 (1986); **34**, 372 (1986); D. B. Graves and K. F. Jensen, IEEE Trans. Plasma Sci. **PS14**, 78 (1986).
[20] J. H. Ingold, in *Gaseous Electronics*, edited by M. N. Hirsh and H. J. Oskam (Academic, New York, 1978), Vol. I, Chap. 2, p. 37.
[21] P. Boeuf and E. Marode, J. Phys. D **15**, 2169 (1982); T. J. Moratz, L. C. Pitchford, and J. N. Bardsley, J. Appl. Phys. **61**, 2146 (1987).
[22] C. K. Birdsall and A. B. Langdon, *Plasma Physics via Computer Simulation* (McGraw-Hill, New York, 1985); R. W. Boswell and I. J. Morey, Appl. Phys. Lett. **52**, 21 (1988).
[23] T. J. Sommerer, W. N. G. Hitchon, and J. E. Lawler, Phys. Rev. A **39**, 6356 (1989); T. J. Sommerer, W. N. G. Hitchon, R. E. P. Harvey, and J. E. Lawler, *ibid.* **43**, 4452 (1991).
[24] M. C. Cavenor and J. Meyer, Aust. J. Phys. **22**, 155 (1969); M. M. Kekez, M. R. Barrault, and J. D. Craggs, J. Phys. D **5**, 253 (1972).
[25] For a recent summary of pulsed H_2 discharge work, see J. Christiansen, in *Physics and Applications of Pseudosparks*, edited by M. A. Gundersen and G. Schaefer (Plenum, New York, 1990), p. 1. See also other papers in this volume.
[26] T. Fugiwara, T. Shimada, and K. Sugita, J. Phys. D **18**, 1101 (1985).
[27] D. A. Doughty and A. Gallagher, Phys. Rev. A **42**, 6166 (1990).
[28] H. N. Chu, E. A. Den Hartog, A. R. Lefkow, J. Jacobs, L. W. Anderson, M. G. Lagally, and J. E. Lawler, Phys. Rev. A **44**, 3796 (1991).
[29] M. A. Lieberman and A. J. Lichtenberg, *Principals of Plasma Discharges and Materials Processing* (Wiley, New York, 1994), Chap. 8.
[30] The terminology breakdown voltage is defined as the minimum voltage required for the "catastrophic" growth of current when the current of initiating electrons approaches zero [3]. Here and throughout this paper we use the term "breakdown voltage" interchangeably with its equivalent, the "zero-current, discharge-maintenance voltage." This voltage can be obtained by extrapolating discharge voltages, such as that shown in Fig. 2, to zero current.
[31] H. Schlumbohm, Z. Naturforsch Teil A **22**, 347 (1967); **22**, 1255 (1967).
[32] Z. Lj. Petrović, B. M. Jelenković, and A. V. Phelps, Phys. Rev. Lett. **68**, 325 (1992).
[33] A. V. Phelps, J. Phys. Chem. Ref. Data **19**, 653 (1990); **20**, 1339 (1991); A. V. Phelps, Bull. Am. Phys. Soc. **35**, 1831 (1990).
[34] C. Barbeau and J. Jolly, J. Phys. D **23**, 1168 (1990).
[35] H. Renner, A. Heisen, and J. Witt, in *Proceedings of the Seventh International Conference on Ionization Phenomena in Gases, Belgrade, 1965*, edited by B. Perović and D. Tošić (Gradvinska, Belgrade, 1966), p. 384.
[36] Z. Lj. Petrović and A. V. Phelps, Phys. Rev. E **47**, 2806 (1993), and unpublished. L. C. Pitchford has pointed out that the capacitance between the electrodes should have been given as 4 pF rather than 40 pF. The circuit capacitance is then about 60 times the electrode capacitance.
[37] G. Frank, Ann. Phys. (Leipzig) **19**, 323 (1967). Although not applied to H_2, other models invoking lateral diffusion loss have recently been published. See S. Holló and B. Nyíri, Acta Phys. Hungarica **72**, 71 (1992); I. D. Kaganovich, M. A. Fedotov, and L. D. Tsendin, Zh. Tekh. Fiz. **64**, 22 (1994) [Tech. Phys. **39**, 241 (1994)].
[38] A. V. Phelps, B. M. Jelenković, and L. C. Pitchford, Phys. Rev. A **36**, 5327 (1987).
[39] S. J. Buckman and A. V. Phelps, J. Chem. Phys. **82**, 4999 (1985); H. Tawara, Y. Itikawa, H. Nishimura, and M. Yoshino, J. Chem. Phys. Ref. Data **19**, 617 (1990).
[40] V. T. Gylys and A. V. Phelps, Bull. Am. Phys. Soc. **33**, 136 (1988); V. T. Gylys, B. M. Jelenković, and A. V. Phelps, J. Appl. Phys. **65**, 3369 (1988).
[41] The dominance of electron excitation of the N_2 391.4-nm band relative to excitation by protons is well known in auroral modeling. See, for example, S. C. Solomon, Rev. Geophys. Suppl. **29**, 1089 (1991).
[42] R. J. McNeal and J. H. Birely, Rev. Geophys. Space Phys. **11**, 633 (1973); B. Van Zyl and H. Neumann, J. Geophys. Res. **85**, 6006 (1980); B. Van Zyl, M. W. Gealy, and H. Neumann, Phys. Rev. A **28**, 2141 (1983).
[43] A. V. Phelps and L. C. Pitchford, JILA Data Center Report No. 27, 1985 (unpublished).
[44] B. M. Jelenković and A. V. Phelps (unpublished).
[45] M. E. Woods, B. J. Hopkins. G. F. Matthews, G. M. McCracken, P. M. Sewell, and H. Fahrang, J. Phys. D **20**, 1136 (1987).
[46] B. M. Jelenković, K. Rózsa, and A. V. Phelps, Phys. Rev. E **47**, 2816 (1993).
[47] A. V. Phelps, Z. Lj. Petrović, and B. M. Jelenković, Phys. Rev. E **47**, 2825 (1993).
[48] Note that for the only available set of correlated voltage, current, and emission data for 3 Torr cm, the current calculated from difference between the applied voltage and the discharge voltage and the series resistance R_2 is not equal to the recorded discharge current at times when the current being discharged by the circuit capacitance C_d is small. We have obtained consistency among the data for Figs. 4(a) and 4(b) by scaling the recorded current values by 2/3. Support for this correction is that then the quasi-steady-state voltage and current values are consistent with the large amount of data shown in Fig. 2.

Note that, although this excess measured current could be caused by current leakage along the quartz wall, there was no comparable current present prior to the pulse at the much higher voltages used at lower pressures. This correction was not required for the data of Fig. 3.

[49] G. Herzberg, *The Spectra of Diatomic Molecules* (Van Nostrand, New York, 1950), p. 554.

[50] Spatial scans are also made with an interference filter peaking near 380 nm in an unconvincing attempt to observe the $H_2(G\,^1\Sigma_g^+ \rightarrow B\,^1\Sigma_u^+)$ band emission. This band is clearly observed in our spectral scans using a monochromator resolution ≈ 1 nm, but our use of broadband (≈ 20 nm) interference filters makes the signal from the uv continuum much stronger relative to the signal from other spectral features than is the case when using the monochromator. See H. M. Crosswhite, *The Hydrogen Molecule Wavelength Tables of G. H. Dieke* (Wiley, New York, 1972), Chap. 1.

[51] B. M. Jelenković and A. V. Phelps, Phys. Rev. A **36**, 5310 (1987).

[52] A. V. Phelps, Bull. Am. Phys. Soc. **38**, 2328 (1993).

[53] Z. Lj. Petrović and A. V. Phelps, Bull. Am. Phys. Soc. **39**, 1490 (1994).

[54] V. I. Kolobov and A. Fiala, Phys. Rev. E **50**, 3018 (1994).

[55] M. A. Biondi, in *Principles of Laser Plasmas*, edited by G. Bekefi (Wiley, New York, 1976), Chap. 4.

[56] B. M. Jelenković and A. V. Phelps, Bull. Am. Phys. Soc. **39**, 1490 (1994).

[57] It should be noted that almost all previous determinations of the thickness of the cathode fall appear to be visual estimates using either direct observation or photographic recording of emission. The distance is that from the cathode to the apparent end of the dark region extending from the cathode toward the anode [3–5]. Given the uncertainties involved in defining this dimension brought out by the present paper for hydrogen and by Ref. [58] for argon, we have taken the thickness of the cathode fall as the distance to the peak of emission in the cathode glow region. The variations of the spatial distribution with spectral feature make this dimension a poor choice for comparison of models with the older data.

[58] K. Rózsa, A. Gallagher, and Z. Donkó, Phys. Rev. E **52**, 913 (1995).

[59] M. A. Folkhard and S. C. Haydon, Aust. J. Phys. **24**, 519 (1971); **24**, 527 (1971).

[60] Z. Stokic, M. M. F. R. Fraga, J. Bozin, V. Stojanović, Z. Lj. Petrović, and B. M. Jelenković, Phys. Rev. A **45**, 7463 (1992).

[61] S. A. Bzenic, S. B. Radovanov, S. B. Vrhovac, and B. M. Jelenković, Chem. Phys. Lett. **184**, 108 (1991).

[62] S. B. Radovanov, K. Dzierżęga, J. R. Roberts, and J. K. Olthoff, Appl. Phys. Lett. **66**, 2637 (1995); S. B. Radovanov, J. K. Olthoff, R. J. VanBrunt, and S. Djurović, J. Res. Natl. Inst. Stand. Technol. **78**, 746 (1995).